Nanoscale Res Lett (2010) 5:1525–1534
DOI 10.1007/s11671-010-9728-5

NANO REVIEW

Hollow Nanostructured Anode Materials for Li-Ion Batteries

Jun Liu · Dongfeng Xue

Received: 28 July 2010 / Accepted: 2 August 2010 / Published online: 13 August 2010

Abstract Hollow nanostructured anode materials lie at the heart of research relating to Li-ion batteries, which require high capacity, high rate capability, and high safety. The higher capacity and higher rate capability for hollow nanostructured anode materials than that for the bulk counterparts can be attributed to their higher surface area, shorter path length for Li^+ transport, and more freedom for volume change, which can reduce the overpotential and allow better reaction kinetics at the electrode surface. In this article, we review recent research activities on hollow nanostructured anode materials for Li-ion batteries, including carbon materials, metals, metal oxides, and their hybrid materials. The major goal of this review is to highlight some recent progresses in using these hollow nanomaterials as anode materials to develop Li-ion batteries with high capacity, high rate capability, and excellent cycling stability.

Keywords Li-ion batteries · Anode · Hollow nanomaterials · Nanotubes · Nanocomposites

Introduction

With great success in the portable electronic sector, Li-ion batteries have been considered the most promising energy storage technology for hybrid, plug-in hybrid, and electric vehicle applications, which are central to the reduction of CO_2 emissions arising from transportation. A Li-ion battery is mainly composed of an anode (negative), a cathode (positive), an electrolyte, and a separator (Fig. 1). Previous studies have showed that there are two categories of cathode materials [1]. One comprises layered compounds with an anion close-packed lattice; transition metal cations occupy alternate layers between the anion sheets and lithium ions are intercalated into remaining empty layers. This kind of electrode materials includes $LiCoO_2$, $LiNi_{1-x}Co_xO_2$, $LiMnO_2$ and $LiNiO_2$. The second group of cathode materials has more open structure, such as vanadium oxides (e.g. V_2O_5), the tunnel compounds of manganese oxides (e.g. MnO_2) and transition metal phosphates (e.g. the olivine $LiFePO_4$). The anode materials include insertion-type materials (such as carbon materials, $Li_4Ti_5O_{12}$, TiO_2), conversion-type materials (such as cobalt oxides, iron oxides, nickel oxides), and alloying-type materials (such as Sn, Si, Ge) [1]. The electrolytes are good ionic conductors and electronic insulators, and most of electrolytes are based on the solution of inorganic lithium salts dissolved in a mixture of two or more organic solvents. The function of the separator is to prevent short circuiting between the anode and the cathode and to provide channels for transportation of Li^+ during the charge/discharge process. On charging, lithium ions are deintercalated from cathode intercalation host, pass across the electrolyte, and are intercalated in the anode such as graphite. Discharge reverses this process (Fig. 1). The electrons pass around the external circuit.

Past decades have witnessed tremendous progress in Li-ion batteries [1–5]; however, there are continuous demands for batteries with higher power and energy density and longer cycling life to power newly emerging electronic devices, advanced communication facilities. As the performance of Li-ion batteries strongly depends on the electrode properties, significant improvements in the

J. Liu · D. Xue (✉)
State Key Laboratory of Fine Chemicals,
Department of Materials Science and Chemical Engineering,
School of Chemical Engineering, Dalian University
of Technology, 116012 Dalian, China
e-mail: dfxue@dlut.edu.cn

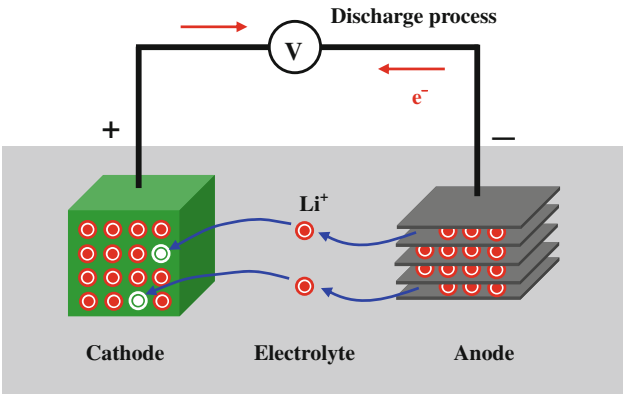

Fig. 1 Schematic representation of a Li-ion battery

electrochemical properties of electrode materials are essential to meet the demanding requirements these applications. One example of this improvement is the rapid development of nanostructured electrode materials [2]. The size reduction into nanoscale leads to increased electrode/electrolyte contact areas and shortened Li^+ transport distance, permitting batteries to operate at higher power. Among these nanostructured materials, hollow nanomaterials, such as hollow micro/nanospheres and nanotubes, are special and unique. Due to their well-defined interior voids, low density, large surface area, and surface permeability, these nanostructured materials have wide applications in a number of areas including Li-ion batteries, catalysts, optoelectronic sensors, drug-delivery carries, and chemical reactors [6–28]. Besides their large surface area and short effective diffusion distance for Li^+, the cavities in hollow structured electrodes for Li-ion batteries may provide extra space for the storage of Li^+, beneficial for enhancing specific capacity. Furthermore, the void space in hollow structures buffers against the local volume change during Li insertion/desertion and is able to alleviate pulverization and aggregation of the electrode materials, hence improving cycling performance. The present article provides a simple overview on the hollow nanostructured anode materials for Li-ion batteries, including carbon materials, metals, metal oxides, and their hybrid materials.

Carbon Materials

Commercial Li-ion batteries usually employ carbonaceous materials as anodes, in which Li^+ is inserted during charging. The resulting Li-interacted carbons exhibit a low potential close to that of metal Li electrode. With carbonaceous materials as anodes, the knotty problems of dendrite formation in the initially employed metal Li anode can be avoided, and the safety of Li-ion batteries are improved greatly. Carbon materials are usually specified into three groups, namely, graphite and graphitized materials, ungraphitized soft carbon, and hard carbon [3]. Graphite is most widely used due to its stable specific capacity (a theoretical capacity of 372 mA h g^{-1}, forming LiC_6), small irreversible capacity, and good cycling performance. Soft carbon materials exhibit a very high reversible Li-storage capacity but a serious voltage hysteresis during delithiation. Hard carbon shows a high Li-storage capacity of 200–600 mA h g^{-1} and good power capability, but poor electrical conductivity and a large irreversible capacity.

To improve the diffusion coefficient of Li^+, Müller et al. designed and fabricated a new type of nanographene-constructed hollow carbon nanospheres (NGHCs) via the precursor-controlled pyrolysis approach [29]. Figure 2a shows the detailed formation procedures for these unique hollow nanostructured carbon anodes. During the fabrication process, they employed discotic nanographenes as building blocks and SiO_2/space/mesoporous SiO_2 nanospheres as templates. The obtained NGHCs exhibit uniform size (about 340 nm in diameter) and thin interior solid walls (70 nm thickness). In the exterior walls of NGHCs, nanochannels arrange perpendicularly to the surface of hollow nanospheres, which is favorable for Li^+ diffusion from different orientations, while the interior graphitic solid walls of these hollow carbon nanospheres can facilitate the collection and transport of electrons during the discharge/charge process (Fig. 2b). When used as anode materials, these NGHCs show a large irreversible capacity of about 1,000 mA h g^{-1} during the first discharge and charge process. After 30 cycles at a rate of C/5 (one Li per six formula units (LiC_6) in 5 h), the reversible capacity is stable at about 600 mA h g^{-1}. Upon increasing the discharge/charge rates to 1C and 5C, its reversible capacities

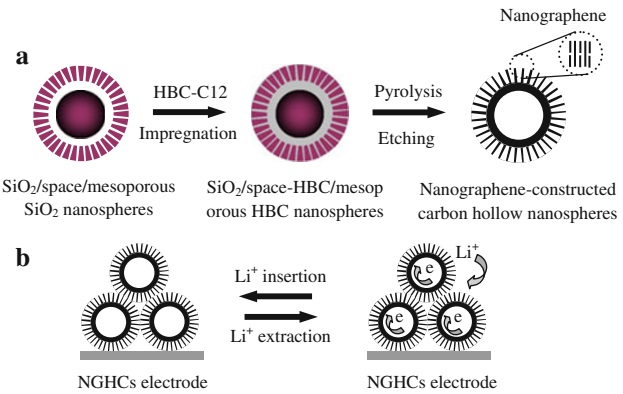

Fig. 2 **a** Schematic presentation of the fabrication of nanographene-constructed hollow carbon nanospheres (NGHCs); **b** diffusion of lithium ions and electrons during charge/discharge processes of the NGHCs electrode. In the exterior walls of NGHCs, nanochannels arrange perpendicularly to the surface of curved nanospheres, which is favorable for Li^+ diffusion from different orientations; the interior graphitic solid walls facilitate the collection and transport of electrons during the cycling process [29]

can be maintained at 390 and 275 mA h g^{-1}, respectively. The high performance of these unique hollow nanostructured carbon materials is ascribed to the high electrical conductivity and rapid charge-transfer reaction for Li^+ insertion and extraction. Song et al. reported the fabrication of hollow grapheme oxide microspheres (HGOSs, 2–10 μm in diameter) from grapheme oxide nanosheets utilizing a water-in-oil emulsion technique [30]. The heat-treated HGOSs exhibit a 485 mA h g^{-1} reversible capacity and high rate performance due to the hollow nanostructure, thin and porous shells consisting of grapheme. Similarly, Zhao et al. reported the fabrication of hollow carbon microspheres with smooth single shells, deformed single shells, double shells, and N-doped shells using SiO_2 microspheres as templates and benzene as carbon precursor via chemical vapor deposition [31]. These hollow carbon microspheres cycled very well after 100 cycles at high current density. Electrochemical experiments also demonstrated that the cyclability of hollow carbon microspheres was improved after doping with N.

Metal Oxides and Composites

Although carbon anode materials have received wide-range applications in Li-ion batteries, it is recognized that graphitic carbon anodes suffer from solvent co-intercalation in propylene-carbonate-based electrolytes, which results in large interlayer expansion and subsequent degradation of structure. Furthermore, the gravimetric and volumetric capacity of carbon materials is limited. The rapid development of electronic devices and electric vehicles demands a much higher energy density. Therefore, some other metal or alloy and transition-metal oxides have been explored as anodes for Li-ion batteries. These transition-metal oxide anodes can be specified into insertion-type materials (such as $Li_4Ti_5O_{12}$, TiO_2) [32–35], alloying-type materials (such as SnO_2, SnO) [36–44], and conversion-type materials (such as Co_3O_4, Fe_2O_3) [45].

Insertion-Type Materials

Among these insertion-type oxide anode materials for Li-ion batteries, $Li_4Ti_{15}O_{12}$ has been considered as one of the most promising alternatives due to its special characters, such as a small volume change during charge/discharge process (zero strain insertion materials), which enables a long and stable cycle life, and a stable insertion potential at 1.55 V versus Li, which avoids the reduction reaction of electrolyte. Additionally, $Li_4Ti_{15}O_{12}$ also has an excellent Li^+ mobility, hence promising for high rate battery applications. Zhou et al. reported the fabrication of $Li_4Ti_5O_{12}$ hollow microspheres by a sol–gel process using carbon microspheres as templates [32]. The $Li_4Ti_5O_{12}$ hollow microspheres show higher Li storage capacity, especially at higher current rates. It is believed that the short Li^+ diffusion distance and large contact area between $Li_4Ti_5O_{12}$ electrode and electrolyte increased both the efficiency of Li^+ and electronic conductivity, hence the rate capability. Jiang et al. prepared hollow spherical $Li_4Ti_5O_{12}$ by the emulsion method [33]. This hollow spheres can be charged/discharged at 20C (3.4 A g^{-1}) with the specific capacity of 95 mA h g^{-1}. Over 500 cycles charge and discharge at 2C, the specific capacity stays very stable at 140 mA h g^{-1} with a loss of 0.01% per cycle. Besides these common hollow spheres of $Li_4Ti_5O_{12}$ anode materials, three-dimensional hierarchical hollow microspheres assembled by thin nanosheets were reported [34]. Hollow structured nanomaterials of other insertion-type oxide materials such as TiO_2 have also been reported [35, 36].

Alloying-Type Materials

Transition-metal oxide anodes based on alloying reaction is another very important kind of anode materials for Li-ion batteries as they show high theoretical capacity. SnO_2-based nanostructured materials have been attracting intensive research attention as high-capacity anodes for a variety of reasons, including their high theoretical capacity, low cost, low toxicity, and widespread availability. A major drawback affects the developing of these materials, that is, the large volume expansion–contraction accompanies the lithium alloying–dealloying or metal reducing and oxidizing process [37, 38, 46]. These volume variations result in severe mechanical strains, which greatly limit the cycling life of electrodes. The use of nanostructured materials is an effective approach for enhancing the rate capability of solid-state electrodes. For example, the hollow or porous nanostructures provide convenient access to Li^+ ingress/egress for reactivity with the active electrode. Archer et al. reported a simple one-pot template-free synthesis of SnO_2 hollow nanospheres, based on an Ostwald ripening mechanism [37]. Through adjusting the polarity of the mixed solvent and precursor concentration, discrete spherical hollow and interconnected hollow core/shell-type SnO_2 nanostructures were prepared with controlled sizes. When used as anode materials, these hollow nanospheres exhibit improved electrochemical properties compared with SnO_2 nanoparticles. Based on this work, they designed a new type of nanoarchitecture, coaxial SnO_2/C hollow nanospheres, which show high cycling performance and rate capability [38]. Figure 3a shows the detailed formation procedures of this unique nanostructure. Firstly, SiO_2 nanospheres were coated with uniform SnO_2. These core/shell SiO_2/SnO_2 nanospheres were then coated with glucose-derived carbon-rich polysaccharide (containing

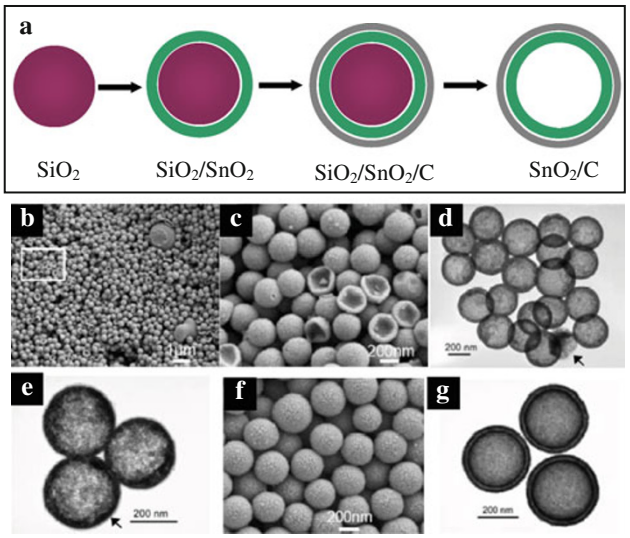

Fig. 3 **a** Schematics of formation of SnO_2/C coaxial hollow nanospheres; **b**, **c** SEM images of SnO_2/C coaxial hollow nanospheres; **d**, **e** TEM images of SnO_2/C coaxial hollow nanospheres; **f** SEM image of double-shelled SnO_2 hollow nanospheres; **g** TEM image of double-shelled SnO_2 hollow nanospheres [38]. Copyright Wiley–VCH Verlag Gmbh & Co. KGaA. Reproduced with permission

abundant hydroxyl groups) by hydrothermal route. Finally, after carbonization, these SiO_2 nanospheres were removed to form SnO_2/C hollow nanospheres. Figure 3b–g shows the morphology and microstructure of these SnO_2/C hollow nanospheres. From Fig. 3d and e, it can be seen that the C shell is tightly attached to SnO_2 shell, which is beneficial for mechanical reinforcement and for enhancing electronic conduction. These hollow nanocomposites deliver a stable capacity of about 210 mA h g^{-1} at a high rate of 4.8C (1C denoted as 625 mA h g^{-1}). After more than 200 cycles at a rate of 0.32C, a stable high capacity of 500 mA h g^{-1} can be resumed.

Recently, Xue group has successfully designed a template-free route for chemical synthesis of SnO_2–V_2O_5 double-shelled nanocapsules [46]. The formation mechanism of these double-shelled hollow nanocapsules is a combination of two types of Ostwald ripening processes (both inward and outward ripening cases), which are shown in Fig. 4 in detail. Ostwald ripening commonly refers to the solution process in which 'the growth of larger crystals from those of smaller size which have a higher solubility than the larger ones' [6, 39, 47, 48]. Inward ripening means that the mass relocation starts from the surface region, while outward ripening refers to the mass transport starting from the center of crystallite aggregate. During the solid hollowing process, because the outer crystallites were loosely packed and/or with smaller crystallite size, crystallites located on the outermost surface of V_2O_3–SnO_2 solid nanospheres would serve as starting points for the subsequent recrystallization process, that is, Ostwald

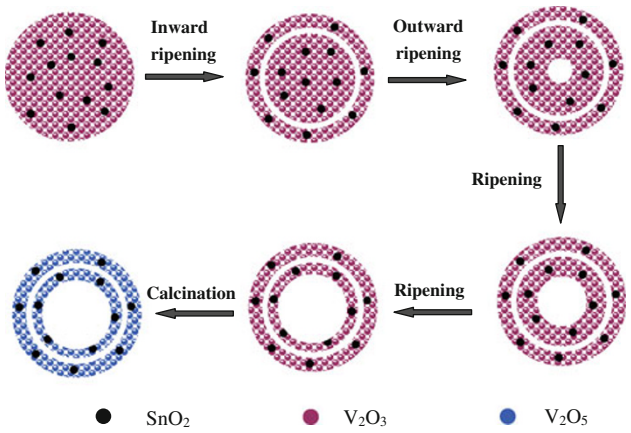

Fig. 4 Schematic presentation of the formation process of V_2O_5–SnO_2 double-shelled nanocapsules based on Ostwald ripening

ripening firstly took place at the surface of these solid nanospheres. Following this inward ripening process, the solid core of nanospheres ripened outward furthermore, leading to double-shelled metal oxide hollow nanocapsules. Finally, double-shelled V_2O_5–SnO_2 nanocapsules were achieved by calcination of these V_2O_3–SnO_2 nanocapsules in ambient air. Figure 5 shows the shape and surface morphology of these nanocomposite nanocapsules. As shown in Fig. 5a, these hollow nanocomposites can be produced on large scale with uniform size and morphology without aggregation. The inset of Fig. 5a is the schematic structure of the double-shelled nanocapsules, which can be confirmed by TEM characterizations. From Fig. 5b–g, it can be seen that these double-shelled nanocapsules have an average diameter of 550 nm, and SnO_2 tiny nanocrystals are homogenously distributed in V_2O_5 matrix (double shells). Figure 6 shows the electrochemical performance of these oxide nanocomposites used as anode materials. These V_2O_5–SnO_2 hollow nanocapsules show a large reversible capacity of 947 mA h g^{-1} (Fig. 6a). After 50 cycles (at a current density of 250 mA g^{-1}), V_2O_5–SnO_2 nanocomposites still can deliver a reversible capacity of 673 mA h g^{-1}, 70% of its initial capacity (Fig. 6b). Additional, these hollow nanostructured composites have a good rate capability as anode material. If the content of SnO_2 is increased in nanocomposites, the reversible capacity as anode electrode can be improved simultaneously. Figure 7 shows the electrochemical characterization of nanocomposites with 15 wt% SnO_2 content. Figure 7a shows the charge/discharge curves of initial 20 cycles for these nanocomposites at a current density of 330 mA g^{-1} in 0.01–3 V. Its first discharge capacity is 1,776 mA h g^{-1}, after 20 cycles, the reversible discharge capacity maintains at 1,046 mA h g^{-1} without obvious capacity fading except for the first cycle (Fig. 7b), larger than that of nanocomposites with 10 wt% SnO_2, which should be ascribed to the existence of more active SnO_2 component.

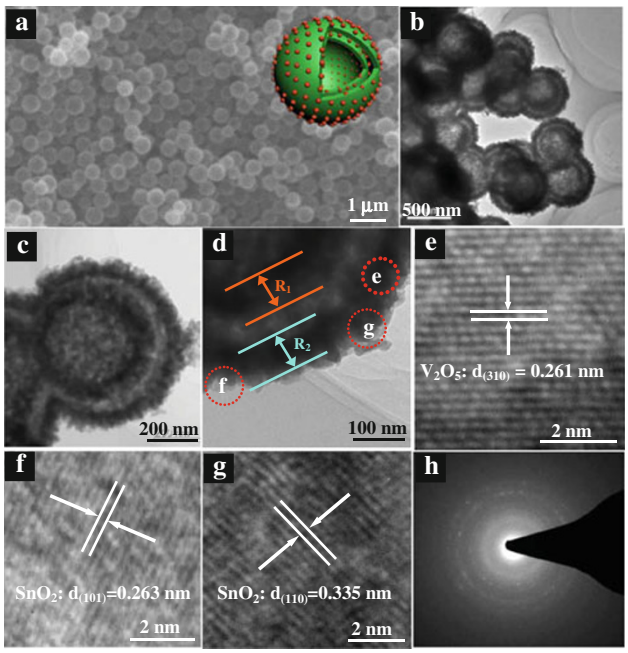

Fig. 5 **a** SEM image of V_2O_5–SnO_2 double-shelled nanocapsules. Inset shows the schematic structure of these double-shelled nanocapsules. The red spheres represent SnO_2 nanocrystals and the green double shells represent the V_2O_5 matrix; **b** low-magnification TEM images; **c**, **d** high-magnification TEM images indicate that the porous shell consists of a great deal of nanocrystals with the thickness of $R_1 \approx R_2 = 90$ nm; **e**–**g** HRTEM images revealing lattice planes of V_2O_5 matrix and SnO_2 nanocrystals; **h** SAED pattern taken from individual nanocapsules which shows that these nanocapsules are polycrystalline. Reproduced with the permission of American Chemical Society from [46]

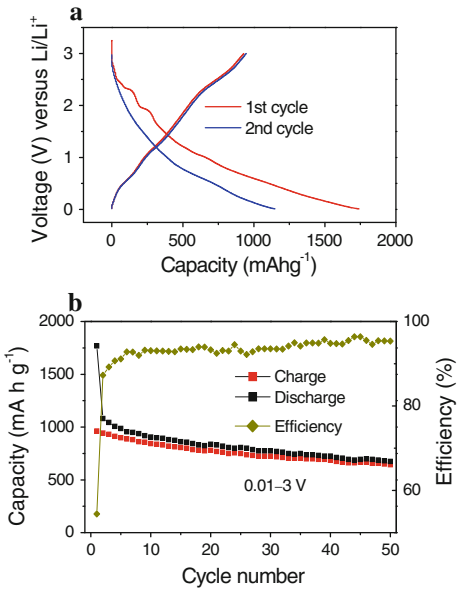

Fig. 6 Anode performance of the as-prepared V_2O_5-based nanocomposites with 10 wt% SnO_2: **a** the first two cycles of charge/discharge curves at a current density of 250 mA g^{-1}; **b** capacity (*left*) and efficiency (*right*) versus cycle number at a current density of 250 mA g^{-1} rate showing the charge and discharge capacity. Reproduced with the permission of American Chemical Society from [46]

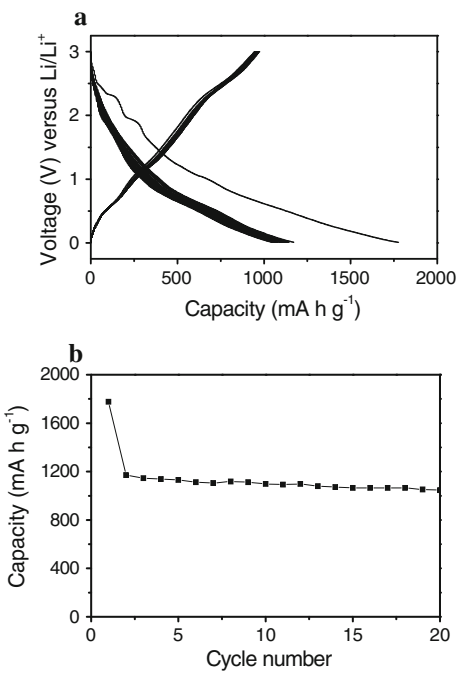

Fig. 7 Anode performance of the as-prepared V_2O_5-based nanocomposites with 15 wt% SnO_2: **a** charge–discharge tests at the current density of 350 mA g^{-1} in the potential window of 0.01–3 V; **b** capacity versus cycle number for V_2O_5–SnO_2 double-shelled nanocapsules at the 350 mA g^{-1} rate

As V_2O_5 is a typical cathode material for Li-ion batteries, we have also tested their cathode performance. Figure 8a shows first two charge/discharge curves of a Li/V_2O_5–SnO_2 cell in the voltage window of 2–4 V at a current density of 50 mA g^{-1}. The first discharge and charge capacities are both around 250 mA h g^{-1} (Fig. 8a), which is close to the theoretical capacity for two Li insertion into V_2O_5 (290 mA h g^{-1}) [4]. At a high current density of 500 mA g^{-1}, these nanocomposites are able to deliver a reversible capacity of about 140 mA h g^{-1}, about 56% of its full capacity. Figure 8b shows the cycle performance of double-shelled nanocapsules between 2 and 4 V at a current density of 100 mA g^{-1} for 50 cycles, indicating a good capacity retention and high columbic efficiency. After 50 cycles, these V_2O_5–SnO_2 hollow nanocapsules deliver a reversible capacity of 174 mA h g^{-1}, corresponding to 82% of its initial capacity (Fig. 8b). Except for the first several cycles, the columbic efficiency for the rest of cycles is always above 99% (Fig. 8b).

In addition to these hollow micro/nanospheres, some one-dimensional hollow structured SnO_2-based nanomaterials have also been synthesized and employed as anodes for Li-ion batteries [42–45]. Qi et al. reported the synthesis of SnO_2 nanotubes with controllable morphologies using a variety of one-dimensional SiO_2 mesostructures (chiral nanorods, nonchiral nanofibers, and helical nanotubes) as

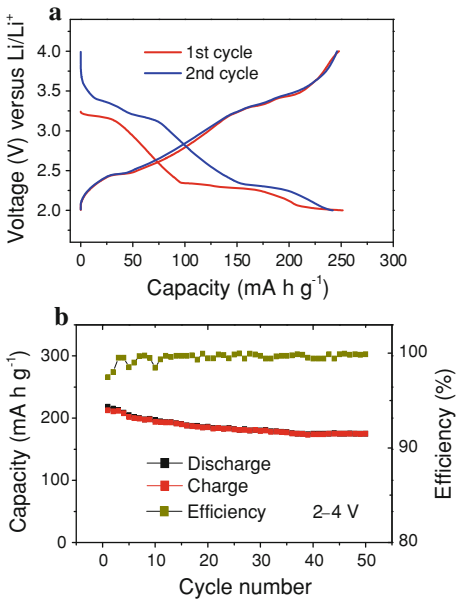

Fig. 8 Cathode performances of the as-prepared V_2O_5-based nanocomposite with 10 wt% SnO_2: **a** the first two cycles of charge/discharge curves at a current density of 50 mA g^{-1}; **b** capacity (*left*) and efficiency (*right*) versus cycle number at a current density of 100 mA g^{-1} rate showing the charge and discharge capacity. Reproduced with the permission of American Chemical Society from [46]

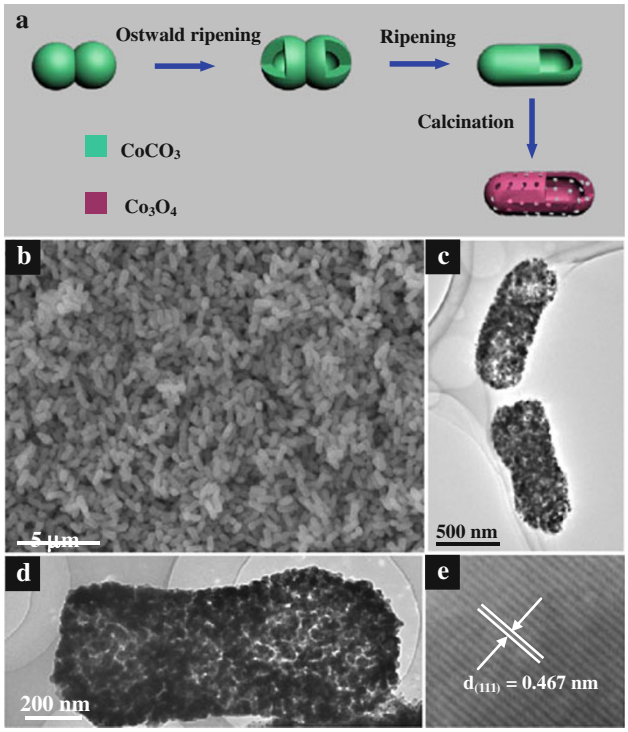

Fig. 9 **a** Schematic presentation of the evolvement process of anisotropic Co_3O_4 porous nanocapsules; **b** low-magnification SEM image showing that these nanocapsules are monodisperse with a uniform size; **c** low-magnification TEM image showing the porous shell of anisotropic Co_3O_4 nanocapsules; **d** high-magnification TEM image exhibiting a single porous Co_3O_4 nanocapsule; **e** HRTEM image of individual nanocrystals revealing the (111) lattice plane

effective sacrificial templates [42]. The as-obtained SnO_2 short nanotubes, which were fabricated with SiO_2 chiral nanorods as templates, show a specific discharge capacity of 468 mA h g^{-1} after 30 cycles. Lee et al. reported the synthesis of C/SnO_2 porous nanotubes through template deposition method with carbon nanotubes as templates [43]. These C–SnO_2 hollow nanocomposites exhibit a reversible capacity of 600 mA h g^{-1} and a good cyclability in Li^+ storage and retrieval.

Conversion-Type Materials

On the other hand, lithium reaction of some 3d transition-metal oxides is a conversion reaction, similar to non-alloy metal oxides, such as Co_3O_4, CuO, and Fe_2O_3 [49], which can be reversibly reduced and oxidized, coupled with the formation and destruction of lithium oxide, respectively.

Recently, Xue group reported a novel self-templated method to synthesized anisotropic Co_3O_4 porous and hollow nanocapsules derived from $CoCO_3$ precursors [49]. The current self-template method is based on inside-out Ostwald ripening. Figure 9a illustrates the self-template transformation process for the synthesis of anisotropic Co_3O_4 porous and hollow nanocapsules from $CoCO_3$ precursors. During the solvothermal process, two aggregated spherical $CoCO_3$ colloids fused together under the driving force of magnetic dipole interaction between these spherical precursor colloids, forming anisotropic dumbbell-like colloids. Subsequently, these newly formed dumbbell-like colloids ripened into column-like colloids. The formation of nanoporous Co_3O_4 shells is attributed to the release of CO_2 from the $CoCO_3$ nanocrystals along different directions. Interestingly, when these column-like precursor colloids were further solvothermally treated, monodisperse spindle-like nanoparticles were achieved. Figure 10 shows the surface morphology and microstructure of spindle-like Co_3O_4 porous and hollow nanocapsules obtained from the corresponding spindle-like $CoCO_3$ precursors. From Fig. 10a, it can be clearly observed that these spindle-like Co_3O_4 hollow nanocapsules have a uniform size or diameter. Some broken hollow nanocapsules can be clearly distinguished, which confirms their hollow character. Furthermore, the hollow nature of the as-prepared spindle-like Co_3O_4 can be further proved by the TEM image (Fig. 10b). The contrast between the central portion and the edge of Co_3O_4 colloids strongly supports the formation of hollow spindle-like colloids. Similar to column-like Co_3O_4 nanocapsules, these spindle-like nanocapsules have nanoporous shells with dense nanopores (Fig. 10c, d). These Co_3O_4 porous nanocapsules should exhibit super Li-ion battery performances

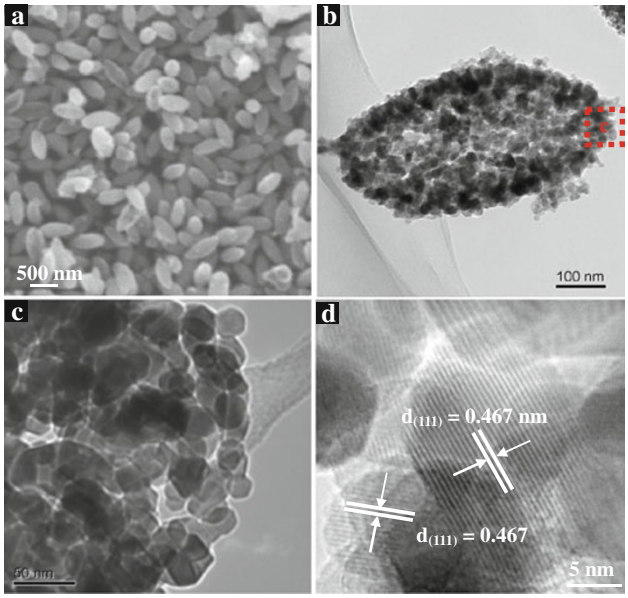

Fig. 10 SEM and TEM characterizations of spindle-like Co_3O_4 porous and hollow nanocapsules: **a** low-magnification SEM image exhibiting that these spindle-like nanocapsules have porous shell; **b** low-magnification TEM image showing a single porous Co_3O_4 nanocapsule; **c** high-magnification TEM image indicates that the porous shell consists of a great deal of Co_3O_4 nanocrystals in the size of ~20 nm. The inset is the SAED pattern taken from a single nanocapsule, indicating that these porous nanocapsules are polycrystalline; **d** HRTEM image of Co_3O_4 nanocrystals revealing the (111) lattice plane

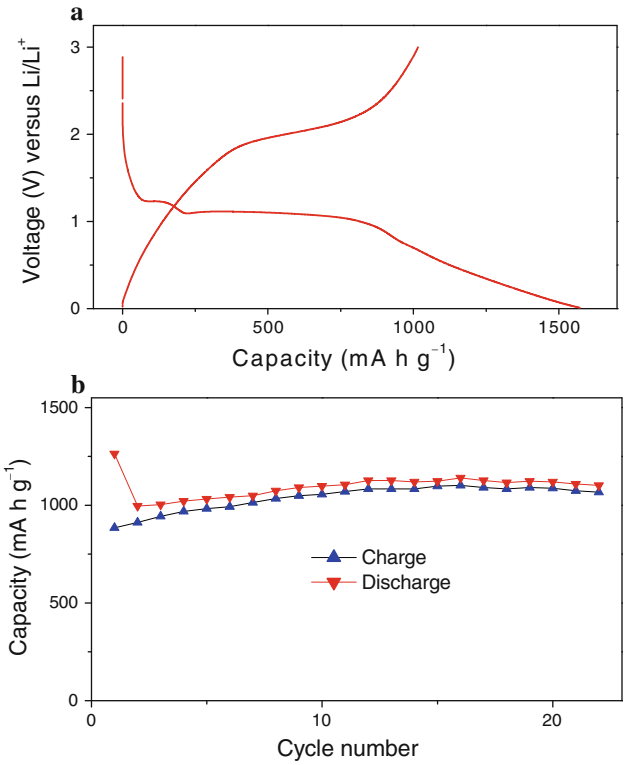

Fig. 11 **a** The first charge–discharge curves of anisotropic Co_3O_4 porous nanocapsules at a current density of 110 mA g^{-1}; **b** cycling performance of Co_3O_4 porous nanocapsules at a current density of 130 mA g^{-1}

with good cycle life and high capacity due to their porous and hollow nanostructures and small size of building blocks. Figure 11a shows the first discharge/charge curves at a current density of 110 mA g^{-1}. These anisotropic Co_3O_4 porous and hollow nanocapsules have a large initial discharge capacity of 1,572 mA h g^{-1} and show a very high reversible capacity of 1,018 mA h g^{-1}. These Co_3O_4 hollow nanocapsules have an excellent cyclability. Except the first cycle (about 1,263 mA h g^{-1}), the other twenty-one cycles almost maintain constant at ~1,000 mA h g^{-1} (Fig. 11b), which shows small irreversible capacity, high reversible capacity and good cycle life.

Similarly, single-, double-, and triple-shelled hollow nanospheres of Co_3O_4 can be prepared with poly(vinylpyrrolidone) (PVP) as soft templates (Fig. 12) [50]. The final Co_3O_4 products were converted from cobalt glycolate through calcination. The first discharge capacities of single-, double-, and triple-shelled hollow nanospheres are about 1,199, 1,013 and 1,528 mA h g^{-1}, respectively. After 50 cycles, the capacity can remain as 680, 866, and 611 mA h g^{-1}, respectively. Archer et al. developed a self-supported topotactic transformation route for synthesis of need-like Co_3O_4 nanotube anode materials (Fig. 13a) [51]. Figure 13b and c shows the low- and high-magnification

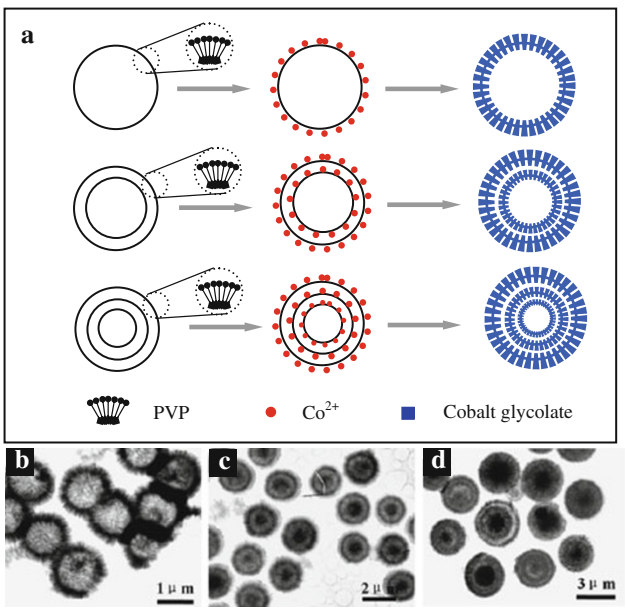

Fig. 12 **a** Schematic presentation fabrication of single-shelled, double-shelled and triple-shelled cobalt precursors in the presence of PVP templates; **b** TEM image of single-shelled cobalt glycolate; **c** TEM image of double-shelled cobalt glycolate; **d** TEM image of triple-shelled cobalt glycolate [50]. Copyright Wiley–VCH Verlag Gmbh & Co. KGaA. Reproduced with permission

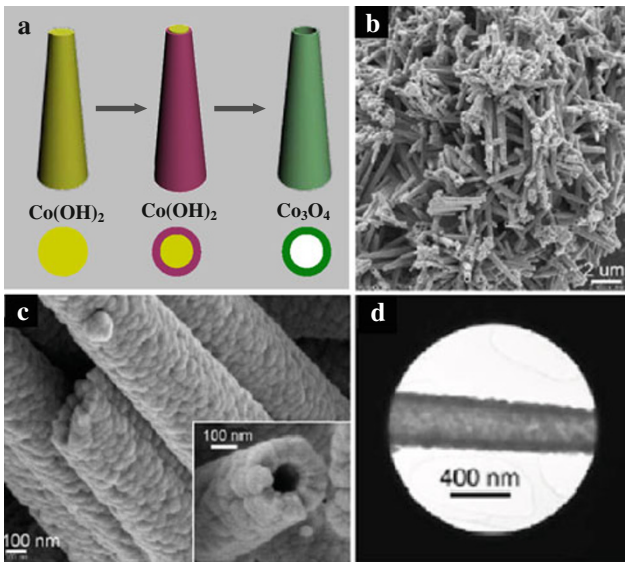

Fig. 13 **a** Schematic presentation of the self-supported topotactic transformation process for formation of needle-like Co_3O_4 nanotubes; **b** low-magnification SEM image of Co_3O_4 nanotubes; **c** high-magnification SEM image of Co_3O_4 nanotubes, the inset shows a cross-sectional view of nanotubes; **d** TEM image of a single nanotube [51]. Copyright Wiley–VCH Verlag Gmbh & Co. KGaA. Reproduced with permission

SEM images of need-like Co_3O_4 nanotube, respectively. It can be clearly observed that these nanotubes with non-constant diameter in the range of 150–400 nm are cylindrical and constructed from Co_3O_4 building blocks of less than 100 nm. These need-like Co_3O_4 nanotubes exhibit a first charge capacity of 950 mA h g^{-1}, and 380 mA h g^{-1} for 80th cycle. Co_3O_4 porous nanotubes derived from $Co_4(CO)_{12}$ on carbon nanotube templates exhibit similar electrochemical performance [52].

Metals and Composites

In order to reduce their irreversible capacity observed in these oxide anodes, oxygen bonded to the electrochemically active metal atom should be avoided. Li alloy–dealloy induces dissociation of the starting materials into active components that will react with Li to form Li-metal alloys. Many metal materials such as Si, Ge, and Sn have been reveled to capable of accommodating Li^+ with both higher Li storage capacities than Li reactive metal oxides and much smaller irreversible capacity [53–62]. Among them, much attention has been focused on Si due to its higher capacity, in spite of its much lower electrical conductivity than other metals [53–56]. Si can alloy with Li up to $Li_{4.4}Si$, corresponding to 4,212 mA h g^{-1} ($4.4\,Li + Si \leftrightarrow Li_{4.4}Si$). However, Si suffers from serious irreversible capacity and poor cyclability, which result from the huge volume swings

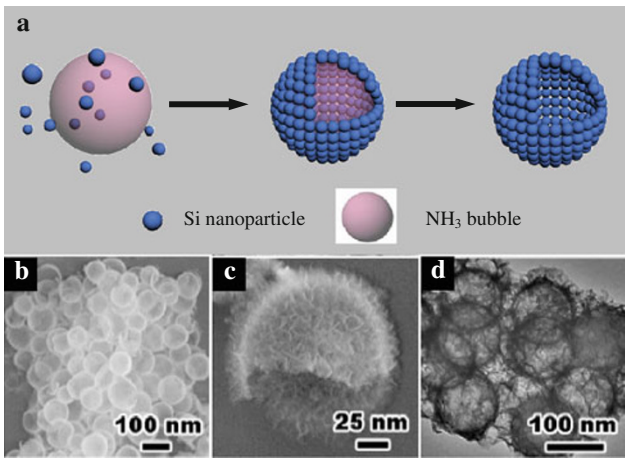

Fig. 14 **a** Schematic illustration of the evolvement process of Si porous nanocapsules with NH_3 as bubble template; **b** low-magnification SEM image of Si hollow nanocapsules; **c** high-magnification SEM image of a typical broken Si hollow nanocapsules; **d** TEM image of Si hollow nanocapsules [53]. Copyright Wiley–VCH Verlag Gmbh & Co. KGaA. Reproduced with permission

during Li^+ insertion/extraction process. This pulverization disadvantage is the disgusting obstacle for practical application of Si as the anode for Li-ion batteries. To overcome this drawback, two strategies have been proposed: using composite materials and forming nanostructured Si-based materials (e.g. Si porous hollow nanospheres). For example, nest-like Si hollow nanospheres were fabricated through solvothermal treatment based on a bubble template (Fig. 14a) [53]. These Si hollow nanospheres are in diameter of 90–110 nm (Fig. 14b) and are composed of ultrahigh and flexural nanowires with the diameter of 5–10 nm (Fig. 14c, d). Due to the three-dimensional hollow nanostructure, these Si hollow nanospheres have high surface area (386 m^2 g^{-1}). These nest-like Si hollow nanospheres display an initial specific capacity of 3,052 mA h g^{-1} at a current density of 2 A g^{-1}. After cycling up to 48 cycles at this current density, the Si nanostructured anode retains 1,095 mA h g^{-1}. With other synthetic methods, some similar hollow nanostructured Sn and Sb anode materials have also been fabricated [57, 58].

For providing conduction paths that are maintained even after pulverization, various metal–C nanocomposites including hollow nanostructures have been achieved through conversion of carbon precursors to amorphous or partially crystalline carbon [59–62]. For example, Sn nanoparticles encapsulated in elastic hollow C nanospheres (TNHCs) were designed based on SiO_2 colloid templates (Fig. 15a) [59]. As shown in Fig. 15c and d, the encapsulated Sn nanocrystals have a diameter of less than 100 nm, and the thickness of C hollow nanospheres is about 20 nm. The void volume (70–80%) and the elasticity of thin C spherical shell can efficiently accommodate the volume change of Sn nanoparticles due to the Li-Sn alloying–dealloying reactions and

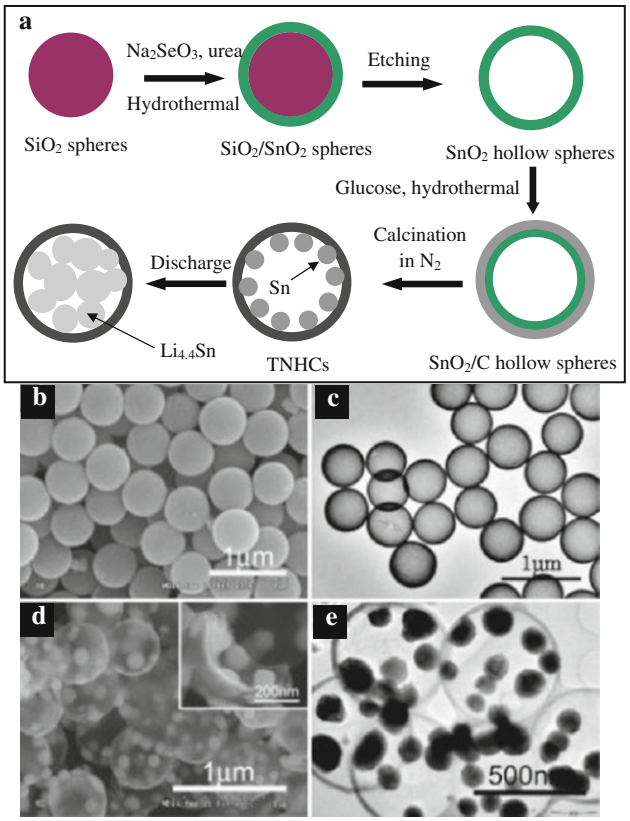

Fig. 15 **a** Synthetic scheme of Sn nanoparticles encapsulated elastic hollow carbon nanospheres (TNHCs); **b** SEM image of SnO_2 coated SiO_2 nanospheres; **c** TEM image of the hollow SnO_2 nanospheres; **d** SEM image of TNHCs, the inset is a close view of a single broken carbon spherical shell studded with Sn nanoparticles; **e** TEM image of TNHCs [59]. Copyright Wiley–VCH Verlag Gmbh & Co. KGaA. Reproduced with permission

thus prevent the pulverization of anode. Testing as anode materials, they have a capacity of >800 mA h g^{-1} in the initial 10 cycles, and >550 mA h g^{-1} after 100 cycles.

Conclusions

The field of nanostructured electrodes for Li-ion batteries is an area of growing interest from both the fundamental and application points of view. In this review, we summarized recent researches in the synthesis and application of hollow nanostructured anode materials used in Li-ion batteries based on carbon materials, metals, metal oxides, and their hybrid materials. Hollow nanomaterials play a great role in improving the performance of Li-ion batteries, because in nanoscale electrodes the distance over which Li^+ diffuses is dramatically shortened; the hollow core can buffer against the local volume change during charge/discharge and provide extra space for the storage of Li^+; and hollow nanomaterials have large surface area and fast diffusion rates along the many grain boundaries existing in hollow nanomaterials. On the other hand, hollow nanostructured materials also have some disadvantages such as high side reactions, low thermodynamic stability, and low volumetric energy density. To gain commercial success of these nanostructured electrodes, however, requires continued fundamental advances in the science and engineering of materials and in fabrication technologies to enable further improved performance.

Acknowledgments The financial support of the National Natural Science Foundation of China (grant nos. 50872016, 20973033) is acknowledged.

References

1. A.S. Arico, P.G. Bruce, B. Scrosati, J.M. Tarascon, W.V. Schalkwijk, Nat. Mater. **4**, 366 (2005)
2. P.G. Bruce, B. Scrosati, J.M. Tarascon, Angew. Chem. Int. Ed. **47**, 2930 (2008)
3. C. Liu, F. Li, L. Ma, H. Cheng, Adv. Mater. **22**, E28 (2010)
4. Y. Guo, J. Hu, L. Wan, Adv. Mater. **20**, 2878 (2008)
5. A. Cao, H. Hu, H. Liang, L. Wan, Angew. Chem. Int. Ed. **44**, 4391 (2005)
6. J. Liu, F. Liu, K. Gao, J. Wu, D. Xue, J. Mater. Chem. **19**, 6073 (2009)
7. C. Yan, J. Liu, F. Liu, J. Wu, K. Gao, D. Xue, Nanoscale Res. Lett. **3**, 473 (2008)
8. J. Liu, D. Xue, Adv. Mater. **20**, 2622 (2008)
9. C. Yan, L. Nikolova, A. Dadvand, C. Harnagea, A. Sarkissian, D.F. Perepichka, D. Xue, F. Rosei, Adv. Mater. **22**, 1741 (2010)
10. C. Yan, D. Xue, Adv. Mater. **20**, 1055 (2008)
11. C. Yan, D. Xue, J. Phys. Chem. B **110**, 7102 (2006)
12. C. Yan, D. Xue, J. Phys. Chem. B **110**, 11076 (2006)
13. C. Luo, D. Xue, Langmuir **22**, 9914 (2006)
14. J. Xu, D. Xue, J. Solid State Chem. **180**, 119 (2007)
15. C. Yan, D. Xue, J. Alloys Compd. **431**, 241 (2007)
16. M. Liu, D. Xue, J. Phys. Chem. C **112**, 6346 (2008)
17. J. Liu, D. Xue, J. Cryst. Growth **311**, 500 (2009)
18. P. Lu, D. Xue, Mod. Phys. Lett. B **23**, 3843 (2009)
19. F. Liu, D. Xue, Mod. Phys. Lett. B **23**, 3769 (2009)
20. M. Liu, D. Xue, Mater. Res. Bull. **45**, 333 (2010)
21. J. Wu, D. Xue, Mater. Res. Bull. **45**, 295 (2010)
22. J. Liu, D. Xue, Nanoscale Res. Lett. (2010). doi:10.1007/s11671-010-9685-z
23. D. Wu, Y. Jiang, J. Liu, Y. Yuan, J. Wu, K. Jiang, D. Xue, Nanoscale Res. Lett. (2010). doi:10.1007/s11671-010-9711-1
24. G. Yang, P. Hu, Y. Cao, F. Yuan, R. Xu, Nanoscale Res. Lett. (2010). doi:10.1007/s11671-010-9658-2
25. G. Shen, D. Chen, Nanoscale Res. Lett. **4**, 779 (2009)
26. B.W. Mwakikunga, A. Forbes, E. Sideras-Haddad, M. Scriba, E. Manikandan, Nanoscale Res. Lett. **5**, 389 (2010)
27. X. Tao, L. Sun, Z. Li, Y. Zhao, Nanoscale Res. Lett. **5**, 383 (2010)
28. J. Kang, Y. Ko, J. Park, D. Kim, Nanoscale Res. Lett. **3**, 390 (2008)
29. S. Yang, X. Feng, L. Zhi, Q. Cao, J. Maier, K. Mullen, Adv. Mater. **22**, 838 (2010)

30. P. Guo, H. Song, X. Chen, J. Mater. Chem. **20**, 4867 (2010)
31. F. Su, X.S. Zhao, Y. Wang, L. Wang, J.Y. Lee, J. Mater. Chem. **16**, 4413 (2006)
32. C. Jiang, Y. Zhou, I. Honma, T. Kudo, H. Zhou, J. Power. Sources **166**, 514 (2007)
33. J. Huang, Z. Jiang, Electrochem. Solid-State Lett. **11**, A116 (2008)
34. Y. Tang, L. Yang, S. Fang, Z. Qiu, Electrochem. Acta **54**, 6244 (2009)
35. X.W. Lou, L.A. Archer, Adv. Mater. **20**, 1853 (2008)
36. G.F. Ortiz, I. Hanzu, T. Djenizian, P. Lavela, J.L. Tirado, P. Knauth, Chem. Mater. **21**, 63 (2009)
37. X.W. Lou, Y. Wang, C. Yuan, J.Y. Lee, L.A. Archer, Adv. Mater. **18**, 2325 (2006)
38. X.W. Lou, C.M. Li, L.A. Archer, Adv. Mater. **21**, 2536 (2009)
39. D. Xu, D. Xue, J. Cryst. Growth **286**, 108 (2006)
40. D. Deng, J.Y. Lee, Chem. Mater. **20**, 1841 (2008)
41. Y. Wang, F. Su, J.Y. Lee, X.S. Zhao, Chem. Mater. **18**, 1347 (2006)
42. J. Ye, H. Zhang, R. Yang, X. Li, L. Qi, Small **6**, 296 (2010)
43. Y. Wang, H.C. Zeng, J.Y. Lee, Adv. Mater. **18**, 645 (2006)
44. H. Zhang, C. Feng, Y. Zhai, K. Jiang, Q. Li, S. Fang, Adv. Mater. **21**, 2299 (2009)
45. J. Chen, L. Xu, W. Li, X. Gou, Adv. Mater. **17**, 582 (2005)
46. J. Liu, H. Xia, D. Xue, L. Lu, J. Am. Chem. Soc. **131**, 12086 (2009)
47. C. Sun, D. Xue, Chemical Bonding Theory of Single Crystal Growth: a Crystallographic Viewpoint, in *Astrophysics and Condensed Matter*, 2nd Quarter, Chap. 8 (Nova Science Publishers, New York, 2008), pp. 215–234
48. X. Yan, D. Xu, D. Xue, Acta Mater. **55**, 5747 (2007)
49. J. Liu, H. Xia, L. Lu, D. Xue, J. Mater. Chem. **20**, 1506 (2010)
50. X. Wang, X. Wu, Y. Guo, Y. Zhong, X. Cao, Y. Ma, J. Yao, Adv. Funct. Mater. **20**, 1680 (2010)
51. X.W. Lou, D. Deng, J.Y. Lee, J. Feng, L.A. Archer, Adv. Mater. **20**, 258 (2008)
52. N. Du, H. Zhang, B. Chen, J. Wu, X. Ma, Z. Liu, Y. Zhang, D. Yang, X. Huang, J. Tu, Adv. Mater. **19**, 4505 (2007)
53. H. Ma, F. Cheng, J. Chen, J. Zhao, C. Li, Z. Tao, J. Liang, Adv. Mater. **19**, 4067 (2007)
54. H. Kim, B. Han, J. Choo, J. Cho, Angew. Chem. Int. Ed. **47**, 10151 (2008)
55. M. Park, M.G. Kim, J. Joo, K. Kim, J. Kim, S. Ahn, Y. Cui, J. Cho, Nano Lett. **9**, 3844 (2009)
56. M. Park, K. Kim, J. Kim, J. Cho, Adv. Mater. **22**, 415 (2010)
57. G. Cui, Y. Hu, L. Zhi, D. Wu, I. Lieberwirth, J. Maier, K. Mullen, Small **12**, 2066 (2007)
58. H. Kim, J. Cho, Chem. Mater. **20**, 1681 (2008)
59. W. Zhang, J. Hu, Y. Guo, S. Zheng, L. Zhong, W. Song, L. Wan, Adv. Mater. **20**, 1160 (2008)
60. Y. Yu, L. Gu, C. Wang, A. Dhanabalan, P.A. van Aken, J. Maier, Angew. Chem. Int. Ed. **48**, 6485 (2009)
61. Y. Yu, L. Gu, C. Zhu, P.A. Van Aken, J. Maier, J. Am. Chem. Soc. **131**, 15894 (2009)
62. K.T. Lee, Y.S. Jung, S.M. Oh, J. Am. Chem. Soc. **125**, 5652 (2003)